In Situ CO_2 and O_2 Measurements on a Profiling Float

BJÖRN FIEDLER

GEOMAR Helmholtz Centre for Ocean Research Kiel, Kiel, Germany

PEER FIETZEK

GEOMAR Helmholtz Centre for Ocean Research Kiel, and CONTROS Systems & Solutions, Kiel, Germany

NUNO VIEIRA AND PÉRICLES SILVA

Instituto Nacional de Desenvolvimento das Pescas, Mindelo, Cape Verde

HENRY C. BITTIG AND ARNE KÖRTZINGER

GEOMAR Helmholtz Centre for Ocean Research Kiel, Kiel, Germany

(Manuscript received 23 February 2012, in final form 12 July 2012)

ABSTRACT

In recent years, profiling floats, which form the basis of the successful international Argo observatory, are also being considered as platforms for marine biogeochemical research. This study showcases the utility of floats as a novel tool for combined gas measurements of CO_2 partial pressure (pCO_2) and O_2. These float prototypes were equipped with a small-sized and submersible pCO_2 sensor and an optode O_2 sensor for high-resolution measurements in the surface ocean layer. Four consecutive deployments were carried out during November 2010 and June 2011 near the Cape Verde Ocean Observatory (CVOO) in the eastern tropical North Atlantic. The profiling float performed upcasts every 31 h while measuring pCO_2, O_2, salinity, temperature, and hydrostatic pressure in the upper 200 m of the water column. To maintain accuracy, regular pCO_2 sensor zeroings at depth and surface, as well as optode measurements in air, were performed for each profile. Through the application of data processing procedures (e.g., time-lag correction), accuracies of floatborne pCO_2 measurements were greatly improved (10–15 μatm for the water column and 5 μatm for surface measurements). O_2 measurements yielded an accuracy of 2 μmol kg^{-1}. First results of this pilot study show the possibility of using profiling floats as a platform for detailed and unattended observations of the marine carbon and oxygen cycle dynamics.

1. Introduction

Accurate knowledge of the interaction of atmosphere and ocean through air–sea gas exchange plays a key role in understanding the past and present states of the global carbon cycle and predicting its future (Takahashi et al. 2009). The ocean's source–sink function for CO_2 can be investigated by measuring the differences of the CO_2 partial pressure (ΔpCO_2) between surface ocean and atmosphere, which is the thermodynamic driving force of the net air–sea exchange (Boutin and Merlivat 2009; Dore et al. 2003; Körtzinger et al. 2008). For many years now, modern observational networks, such as time series and voluntary observing ships (VOSs), have contributed high-quality data to the global assessment of ΔpCO_2 (e.g., Takahashi et al. 2009; Watson et al. 2009). The most comprehensive dataset has recently been published in the Surface Ocean CO_2 Atlas (SOCAT), which contains nearly 7 million shipborne underway measurements of CO_2 in the surface ocean (Pfeil et al. 2012). Despite the growing database, the present global uptake rate of the World Ocean for anthropogenic CO_2 still has an uncertainty of 50% ($+2.0 \pm 1.0$ Pg C yr^{-1}; Takahashi et al. 2009), which to a major extent is due to limited temporal and spatial coverage of large parts of the oceans, for example, the Southern Ocean.

Corresponding author address: Björn Fiedler, GEOMAR Helmholtz Centre for Ocean Research Kiel, Düsternbrooker Weg 20, 24105 Kiel, Germany.
E-mail: bfiedler@geomar.de

DOI: 10.1175/JTECH-D-12-00043.1

Dissolved CO_2 in the ocean is not only influenced by physical processes (e.g., warming/cooling, mixing) but also by biological processes (e.g., photosynthesis, bacterial oxidation of organic matter) and thus strongly linked to dissolved O_2. The exchange of both gases at the ocean–atmosphere interface is rather decoupled from each other due to complex processes in the ocean, such as the chemistry of the carbonate system (Keeling et al. 2010) and their markedly different equilibration time scales. Knowledge of combined air–sea fluxes of O_2 and CO_2 can help to better understand and constrain atmospheric and oceanic tracers such as atmospheric potential oxygen (Stephens et al. 1998) and ocean potential oxygen (OPO) or C* (Keeling et al. 2010; Gruber et al. 1996). Besides the above-named gas exchange processes at the air–sea interface, dynamics at the boundary of the mixed layer and the subsurface layer (e.g., entrainment of respiratory signals from subsurface waters into the mixed layer) play an important role in the understanding of carbon cycling (Gruber et al. 2010b). To investigate these processes, combined measurements of CO_2 and O_2 throughout the entire upper-water column (including the thermocline) are needed. Existing autonomous methods focus either on the ocean surface layer (VOS, buoys) or are performed at fixed locations and water column depths (moorings) and therefore are not capable of operating at high vertical resolution and in remote areas. While mixed layer and subsurface dynamics cannot be observed by these approaches at the desired resolution in space and time, profiling floats and gliders as new observation platforms have started to fill this gap.

The most sophisticated and ambitious project of the international research community to enhance spatiotemporal resolution of observations is the Argo network, consisting of >3000 autonomous profiling floats distributed over the oceans (Roemmich et al. 2009). Nowadays, this physical oceanographic observatory is used more and more by biogeochemists since novel sensors for the measurement of biological and chemical parameters have started to meet the requirements of deployment on profiling floats (e.g., low power consumption, small size, high accuracy, and long-term stability). Early pilot studies for O_2 measurements from this platform (Körtzinger et al. 2004; Riser and Johnson 2008) have demonstrated the utility of floats for biogeochemical studies and thus pushed forward the effort to augment the Argo float observatory with oxygen measurements (Gruber et al. 2010a). Other pilot studies have further demonstrated a broad range of measurements on floats, such as gas tension, turbidity, fluorescence, and nitrate (Johnson et al. 2010; Boss et al. 2008; D'Asaro and McNeil 2007; Bishop et al. 2004).

In contrast to these developments, accurate and precise measurements of pCO_2 have for a long time been restricted to relatively large experimental setups (Körtzinger et al. 1996; Pierrot et al. 2009). The first operational sensor for autonomous in situ pCO_2 measurements (DeGrandpre et al. 1995; Moore et al. 2011) has been used primarily in long-term observations on buoys and moorings at various fixed depths. Because of its semicontinuous measurement principle and rather long equilibration time scale, however, this instrument is not suitable for profiling applications on conductivity–temperature–depth (CTD) rosette water samplers, floats, and on other profiling platforms.

The demand for a new generation of pCO_2 sensors that can extend the present high-quality observations in time and space has fostered many recent developments within the scientific community (Byrne et al. 2010). One of the first small-sized in situ sensors is the HydroC sensor (CONTROS GmbH, Kiel, Germany), which can be deployed at pressures up to 6000 dbar. Power consumption and response time of the instrument as well as size and design of its housing enable this sensor to be deployed on autonomous platforms with limited space and energy availability, such as moorings, floating buoys, or profiling floats (Fietzek et al. 2011).

Here, we present results from an extensive field evaluation of a newly developed profiling float that for the first time was equipped with both an O_2 and pCO_2 sensor. First, we introduce instrumentation design, operational modes, and data processing. Then, we present sensor performance and assess the consistency and reliability of the obtained pCO_2 data. Finally, we examine the possibility of drift control and in situ calibration of the optode data by atmospheric measurements.

2. Methods

a. Float platform

A Navigating European Marine Observer profiling float (NEMO; Optimare GmbH, Bremerhaven, Germany) was used as a sensor carrier for this investigation (Fig. 1). This float's main design is based on the Sounding Oceanographic Lagrangian Observer float (SOLO; Davis et al. 2001). As typical for the Argo network, the NEMO float is equipped with a CTD unit (SBE 41, Sea-Bird Electronics Inc., Bellevue, Washington), Argos telemetry, and an oil and air bladder for buoyancy control. The latter is inflated when the float approaches the surface, thereby further significantly increasing the float's buoyancy and pushing the top cap, including sensors and telemetry, above the water level.

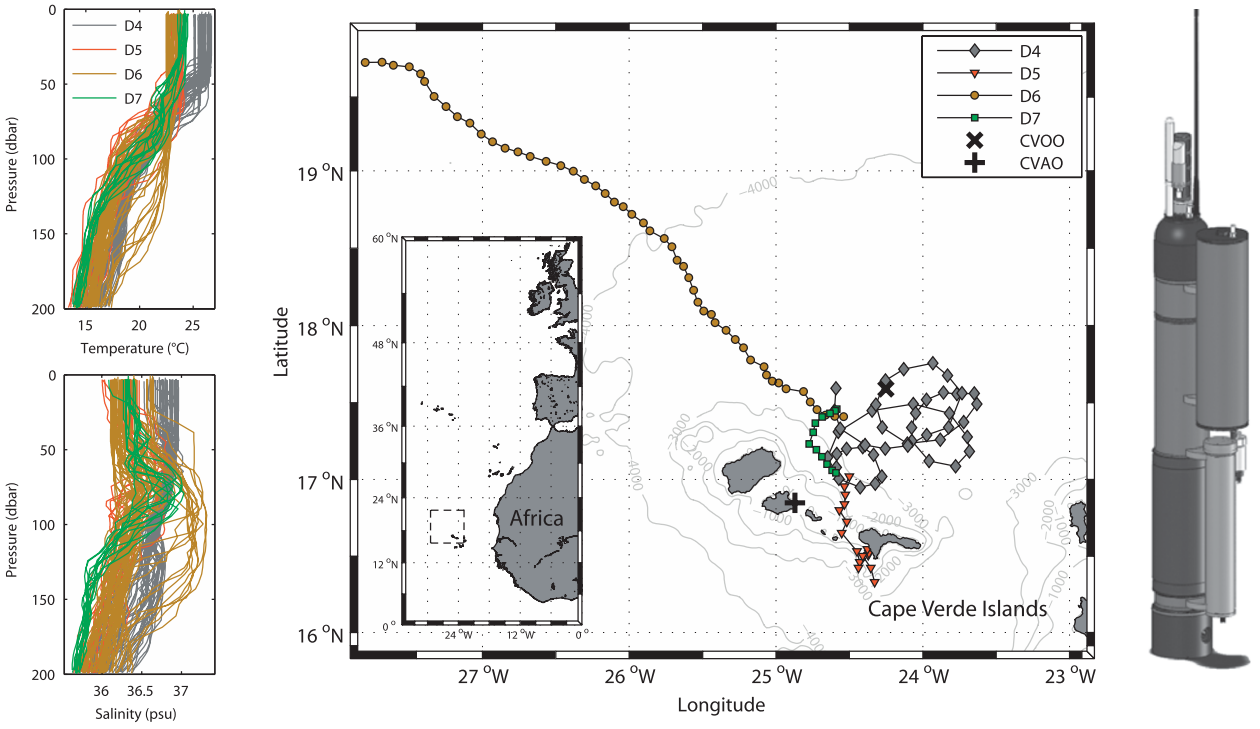

FIG. 1. (left) Depth profiles recorded by the profiling float for (top) temperature and (bottom) salinity during all four deployments. Water masses in the study area were affected by submerged waters originating in the North Atlantic subtropical gyre, as indicated by pronounced subsurface maxima of salinity (Stramma and Schott 1999). (middle) Map shows float trajectories for deployments D4–D7 carried out between November 2010 and June 2011 near the Cape Verde Islands off the coast of Mauritania. Black symbols indicate the location of the CVOO (×) as well as the CVAO (+). Gray contour lines show the ocean bathymetry obtained from the General Bathymetric Chart of the Oceans (GEBCO) dataset. The inset shows the location of the islands with regard to the African mainland. (right) Drawing shows Argo-type profiling float (Optimare GmbH) equipped with a HydroC pCO_2 sensor (including SBE 5M pump), an extra battery container above, an optode sensor, and Iridium and Argos telemetry.

The float underwent several modifications for enabling it to carry further sensor payload and functionality. Argos and Iridium (including GPS) telemetry for bidirectional communication between operator and instrument as well as underway software adaptations ensured full remote control during operations in the field. An O_2 sensor (model 4330 optode, Aanderaa Data Instruments AS, Bergen, Norway) was mounted next to the CTD. The optode sensor was chosen because of its small dimension, low energy consumption, and long-term stability. It has been used successfully in former studies on autonomous platforms (Körtzinger et al. 2005; Tengberg et al. 2006; Johnson et al. 2010).

Additionally, a HydroC pCO_2 sensor (CONTROS) fitted with a pump (SBE 5M, Sea-Bird Electronics) and a depth rating of 2000 dbar was attached to the side of the float with a vertical distance of 1 m to the sensor package described above. This sensor features a planar membrane interface fitted with a flow-through head that is continuously flushed with ambient seawater during measurement. CO_2 along with other dissolved gases as well as water vapor permeates the membrane and equilibrates with the inner pumped gas circuit, where it is quantified by a temperature-stabilized, single-beam, dual-wavelength nondispersive infrared (NDIR) detector. For zeroing [zero-point measurement (ZP)] of the NDIR detector, a CO_2-free gas stream can be produced by passing the air through an internal soda lime cartridge that scrubs the CO_2. The ZPs represent a measure of the actual sensor's performance and are used to account for a zero drift, which is a common and the dominant cause for response change in NDIR instruments (Eckles et al. 1993; McDermitt et al. 1993; P. Fietzek et al. 2013, unpublished manuscript). All ZPs obtained over the course of deployments are considered during post-processing, and the sensor's ZP at any point in time is derived through linear interpolation of the initial ZPs. Furthermore, the signal recovery to ambient pCO_2 levels after a ZP interval is used to derive the actual response time of the sensor, as discussed later in more detail.

To provide energy to the HydroC and the water pump as well as to maintain sufficient buoyancy for the whole float, a battery container was mounted on the side of the float above the HydroC (see Fig. 1). A total of 16

primary lithium battery cells with an overall nominal capacity of 749 Wh were placed in the container, yielding sufficient energy for 39–44 pCO_2 profiles, depending on environmental conditions and configuration. Design and payload of this container result in positive buoyancy and thereby stabilize the vertical orientation of the float. Battery capacity for the remaining components (telemetry, buoyancy control, CTD, and optode) was designed for 150 profiles (1152 Wh in total) and placed in the main pressure housing of the float according to a configuration used for standard Argo floats.

b. CO_2 and O_2 sensor calibration

Prior to the first deployment, the HydroC and optode sensors were thoroughly calibrated in the laboratory. For this purpose, the HydroC sensor was submerged into a thermally insulated and closed water bath, wherein ambient pCO_2 values were varied at different temperatures between 200 and 800 μatm by changing the carbonate system in the bath (P. Fietzek et al. 2012, unpublished manuscript). A high-precision, classical, equilibrator-based pCO_2 system (Körtzinger et al. 1996), equipped with a CO_2 sensor (model 6262, LI-COR Inc., Lincoln, Nebraska) calibrated regularly against National Oceanic and Atmospheric Administration (NOAA)-certified standard gases, served as a reference system for the tank's pCO_2, thus providing an accuracy of 2–3 μatm, which is typical for these instrumental setups (Pierrot et al. 2009).

The optode sensor was calibrated with a recently developed high-accuracy electrochemical calibration setup for O_2 sensors (Bittig et al. 2012). Calibrations were done at stable and well-defined electrochemically generated dissolved O_2 concentrations in a flow system where the sensor was submerged into a thermally insulated water bath and the sensor head was attached to a miniaturized flow-through cell. Calibration was performed covering a temperature range from 8° to 25°C. Overall, seven calibration points between 129 and 317 μmol kg^{-1} O_2 were recorded and triplicate Winkler samples used as reference. Additionally, three zero oxygen measurements using sodium sulfite were performed within the calibration's temperature range. The optode's batch foil coefficients were refitted after Uchida et al. (2008), and all 10 laboratory calibration points were used for the raw phase calibration. Instead of the standard linear correction [Eq. (1)], Eq. (2) was used, resulting in an overall sensor accuracy of 1.2 μmol kg^{-1} (rmse) from the laboratory calibration, defined as

$$\mathrm{CalPhase} = A + B \times \mathrm{TCPhase}, \quad (1)$$

$$\mathrm{CalPhase} = A + B \times \mathrm{TCPhase} + C \times T_{\mathrm{opt}}, \quad (2)$$

where A, B, and C are fitting parameters, TCPhase is the raw sensor signal, T_{opt} is the sensor's temperature probe, and CalPhase is the laboratory-calibrated sensor signal.

c. Float operations

Unlike the common method of using an Argo float as a disposable device, we pursued an approach that included instrument recovery at the end of each mission. For the purpose of this study, we thereby achieved the following advantages: (i) the regular exchange of batteries enables the float to carry a sensor payload with enhanced power consumption and record data at a higher sampling rate; (ii) internally stored high-resolution data can be downloaded after each mission and are valuable for accurate postprocessing (e.g., profile hysteresis correction); (iii) identified suboptimal performance and (peripheral) malfunctions occurring during one deployment can potentially be fixed immediately, either via remote control access or rapid recovery; (iv) the instrument can be kept in the area of prime interest by timely recovery and subsequent redeployment; and (v) most importantly, sensor drift, and thus accuracy, can be monitored and corrected for properly with pre- and postdeployment calibrations.

The float with the sensor package described above was deployed 4 times between November 2010 and June 2011. During all of these deployments, this setup performed successfully and allowed for a detailed analysis of both the platform's and the sensor's performance (Table 1). All deployments were conducted in the vicinity of the Cape Verde Ocean Observatory (CVOO; 17.589°N, 24.252°W; http://cvoo.geomar.de) in the eastern tropical North Atlantic (ETNA) in close proximity to the Cape Verde Atmospheric Observatory (CVAO; 16.864°N, 24.867°W), which is located downwind of the study area (Fig. 1). Vertical profiles of salinity, temperature, hydrostatic pressure, pCO_2, and O_2 for the upper 200 m of the water column were measured every 31 h during upcasts with a mean ascent speed of 0.06 m s^{-1} and a vertical resolution of 5 dbar [low-resolution (LR) data]. Further, pCO_2 data were recorded in 5-s intervals during upcasts that correspond to a vertical resolution of ~0.3 dbar [high-resolution (HR) data]. At the parking depth of ~250 dbar and immediately before each profile, the float initializes a warm-up phase for the HydroC followed by a ZP. Directly after profiling to the surface, a second ZP is carried out. During the time of the second ZP, O_2 measurements are conducted, first in water and then in air. Measurements in air for in situ postcorrection of O_2 data (section 3c) were done after the float had inflated an air bladder and thus pushed the optode sensor, CTD, and telemetry–GPS antenna above water level. Once measurements were finished, LR data

TABLE 1. Field campaigns conducted and data obtained during 2010 and 2011 that form the basis of this study. Former deployments (D1–D3) were disregarded, since these were performed with a different float setup, that is, a different pCO_2 sensor that showed comparatively poor performance and did not allow for the measurement of continuous pCO_2 profiles. Duration of and gaps between consecutive deployments varied because of limited ship resources on site. The asterisk (*) indicates that the instrument got lost during deployment for unknown reason and thus no HR data are available for D7.

				No. of individual measurements		
ID	Deployment time	No. of profiles	Duration (days)	*T*, *S*, *P*	O_2	pCO_2
D4	Nov 2010–Jan 2011	44	56	2200	2200	31 223
D5	Jan–Feb 2011	16	21	800	800	17 489
D6	Mar–May 2011	51	65	2550	2550	42 253
D7	May–Jun 2011	12	14	600	600	600*
Total		123	156	6150	6150	91 565

and GPS location were telemetered to shore via the Iridium network. The dwell time at the surface was less than 1.5 h. Float missions are typically designed for durations of 2 months, but they can be extended depending on sampling frequency and sensor–battery payload.

d. Data processing

Calibrations described in section 2b were applied on recorded raw pCO_2 and O_2 sensor data. Sensor drift was taken into account for each profile by using the information from pre- and postprofile ZPs for the HydroC and atmospheric O_2 measurements for the optode, respectively. Oxygen concentration was derived from raw phase measurement (TCPhase), CTD temperature (T_{CTD}), and atmospheric pressure (recorded at nearby CVAO) using the laboratory calibration. For computation of O_2 measurements in air, values of the optode's temperature probe (T_{opt}) were used since these showed a lower noise level in air than T_{CTD}. In absence of steep temperature gradients, both temperature probes, T_{opt} and T_{CTD}, have shown no detectable deviation of each other (<0.01°C). Subsequently, all LR data were merged in the time domain onto the HydroC HR grid by linearly interpolating O_2, salinity (*S*), T_{CTD}, and pressure (*P*).

The response time of membrane-based sensors is a major constraint for profiling platforms (Edwards et al. 2010; Miloshevich et al. 2004). Although the float platform of this study is a rather slow profiling device, the HydroC response time is causing an appreciable hysteresis in obtained vertical pCO_2 profiles. Laboratory- and field-based experiments with the HydroC sensor have shown pronounced changes in sensor response time that linearly depends on water temperature (P. Fietzek et al. 2013, unpublished manuscript). Pressure vessel tests under different isothermal conditions have shown no significant effects of hydrostatic pressure up to 2000 dbar on sensor response time (data not shown here). Sensor response time in pumped mode further depends on the water flow rate provided here by an SBE 5M pump. The actual in situ response time of the HydroC was determined by making use of the signal recovery after a ZP directly before (at depth) and after (at surface) each profile. Since the major volume of the inner gas stream is flushed with zero gas during ZP, the sensor needs a distinct time to fully reequilibrate to ambient pCO_2 afterward. Following the initial change after a ZP, which is mostly due to the mixing of the internal gas volumes (zero gas and equilibrated gas behind the membrane), the pCO_2 increase within the inner volume is determined only by the permeation of CO_2 from the water through the membrane layer. The time required for the mixing process is much shorter than the time constant of the permeation process that essentially follows first-order kinetics. Therefore, sensor response time can be assessed by applying an exponential fit to the signal increase following the short mixing interval after a ZP using Eq. (3), given as

$$\text{signal}(t) = (a - b)e^{-\Delta t/\tau} + b, \tag{3}$$

where a is the sensor signal for the well-mixed internal gas volume during ZP, b is the sensor signal after the measurement has reequilibrated with ambient pCO_2 levels, τ is the reciprocal *e*-folding response time, and Δt is the relative time domain between a and b. Next, a, b, and τ are derived as fitting parameters by an exponential fit (nonlinear least squares). This approach provides a sensor response time for every single measurement during an upcast, based on the two in situ determinations of the response time in combination with its determined linear dependence on water temperature. Further, this approach also accounts for other effects on sensor response time, such as potential biofouling, changes in water flow to the membrane, or other physical effects (e.g., pressure conditioning) on the membrane's structure that may develop during the course of a deployment.

A time-lag correction algorithm (Miloshevich et al. 2004) has been applied on carefully smoothed vertical

HR profiles of pCO_2 that takes varying response times of the HydroC with ambient conditions into account. By knowing sensor behavior and the exact time stamp for each measurement, one can apply the following model sequentially to time-lagged data:

$$U_C(t_1) = \frac{U_M(t_1) - [U_M(t_0)e^{-\Delta t/\tau}]}{1 - e^{-\Delta t/\tau}}, \quad (4)$$

where $U_M(t_0)$ is the measured value at the first time stamp; $U_M(t_1)$ is the measured value at the following time stamp; Δt is the time between t_0 and t_1; and $U_C(t_1)$ is the time-lag-corrected (TLC) measurement at t_1, referred to as TLC data. To meet the requirements for the application of such a correction algorithm, one has to provide a sufficiently small sampling rate Δt relative to the response time and expected gradients (Miloshevich et al. 2004). HR data for pCO_2 fulfill these conditions and thus allow a careful application of this algorithm in order to examine the performance of pCO_2 measurements properly.

Response time of the optode sensor is about an order of magnitude faster than the HydroC as deployed here and laboratory experiments also show a distinct dependence of the response time on water temperature in a stationary setup (H. C. Bittig et al. 2013, unpublished manuscript). However, since an in situ determination of optode response times was not feasible and the originally recorded optode data (LR data) provide only an insufficiently short sampling interval, no TLC data could be derived from these measurements (refer to section 3c for further details).

e. Reference data

For validation of sensor accuracy and data processing described in section 2d, independent observations such as shipborne field tests in case of the HydroC sensor, hydrocast data in close proximity to float operations, and a global climatology have been used.

First, a similar HydroC sensor setup was tested during a hydrographic survey in the equatorial Atlantic in order to validate the applied correction algorithm on sensor output. The device was mounted on a CTD rosette equipped with an O_2 sensor (SBE43, Sea-Bird Electronics Inc.) and multiple upcasts and downcasts were performed. During the final upcast, discrete water samples for dissolved inorganic carbon (DIC) and total alkalinity (TA) were collected. Analysis of these samples was carried out immediately after sampling by using automated high-precision analyzing systems [single-operator multimetabolic analyzer (SOMMA) for DIC, Johnson et al. (1987); versatile instrument for the determination of titration alkalinity (VINDTA) for TA, Mintrop et al. (2000)]. Accuracy and precision of these discrete measurements were assured by regular analysis of certified reference material (CRM; A. Dickson, Scripps Institution of Oceanography, La Jolla, California; Dickson 2010) and duplicate samples, respectively. DIC (± 0.9 μmol kg^{-1}) and TA (± 1.9 μmol kg^{-1}) measurements were converted into pCO_2 for comparison purposes, using the carbonic acid dissociation constants of Mehrbach et al. (1973) refit by Dickson and Millero (1987). Because of uncertainties in the used set of constants and in the DIC and TA measurements, the uncertainty of derived pCO_2 reference values is estimated to be ± 10 μatm (Millero 2007). Additionally, a fully automated pCO_2 measurement system [General Oceanics (GO), Miami, Florida] based on a spray head equilibrator and a CO_2 analyzer (model 6262, LI-COR Inc.) was operated in parallel during CTD tests. Data reduction procedures were applied after Pierrot et al. (2009).

Second, for comparison purposes, DIC, TA, and O_2 (Winkler method) data from ship expeditions in the vicinity of the study area were used. Furthermore, reference samples were taken immediately prior to the fourth and seventh deployment of the float (D4 and D7, respectively) in a distance of less than 100 m to the point of deployment. DIC and TA samples (500 mL) were preserved by poisoning with 100 μL of saturated mercury chloride solution, and onshore analysis was conducted following the procedures described above.

Third, float pCO_2 data obtained at the surface were compared with a global climatology (Takahashi et al. 2009) for a qualitative assessment of data reliability for the respective region and time of year. Climatology data were extrapolated to the time of float operations while taking into account an annual mean pCO_2 increase of 1.8 μatm in the mixed layer in this particular region.

3. Results and discussion

a. CO_2 sensor performance

The HydroC CO_2 sensor is a newly developed device that has recently become available for diverse marine research applications (Fietzek et al. 2011). Hence, this work provides some of the first field data acquired with this sensor, being deployed on a demanding platform. Other field surveys with this sensor (e.g., shipborne underway measurements) demonstrate an overall accuracy of about 5 μatm (P. Fietzek et al. 2013, unpublished manuscript). In case of measurements at nonequilibrium conditions caused by, for example, fast and large changes in water temperature or dissolved gas composition, as commonly present during profiling applications, accuracy might differ and has to be specified for each platform explicitly.

The use of a membrane-based NDIR sensor on autonomous profiling devices is a rather challenging task in terms of measurement stability and reliability under the tight constraints of limited energy resources and steep temperature gradients that are encountered during vertical profiling. Zero values show only a small and comprehensible drift over the course of each deployment, with a maximum drift rate of 0.15 μatm day^{-1}, indicating that the sensor behaves in a stable and rather predictable way (Fig. 2). Even between consecutive deployments (including several weeks of storage without operation), no major change in the drift behavior was found. Also, for individual upcasts, the NDIR sensor signal was not subject to any significant drift. The latter finding is quite remarkable since during upcasts, the sensor experiences major changes in temperature and pressure over a very short time interval (~1.5 h), including a cold start and warm-up phase prior to each profile. This consistency of ZPs at surface and depth illustrates a high degree of sensor robustness and reliability under the encountered conditions. Temporal stability of the sensor response slope (span drift) could not be quantified in this study because of the lack of a postdeployment calibration. However, a comparison with reference samples shows no indication for a pronounced drift in the sensor response slope (section 3b).

The float enters the euphotic zone several times during a deployment. However, it spends about 80% of its full cycle time beneath it until the next profile starts. Although such an observational approach is not prone to major biofouling, adverse effects of this cannot be fully ruled out. For instance, a growing film of organic matter on the membrane interface would first and foremost decrease the membrane's permeability and thus slow down the sensor's response time. In addition, pCO_2 data could be biased because of biological production/respiration processes in this film. To account for the former process, in situ sensor response time was derived after every ZP. Figure 2 presents the observed in situ response times after each profile at the surface (black symbols, k_s) and prior to each upcast at depth (gray symbols, k_d). At the beginning of D4, this CO_2 sensor was deployed in the field the first time and thus experienced its first cycles of rapid temperature and hydrostatic pressure changes. The observed decreasing trends during D4 in both k_d and k_s seem to be indicative of a membrane conditioning phase, which has been observed for membrane-based instrumentation during former studies (Marin et al. 1992; Baudot et al. 1999; McNeil et al. 2006). The elevated scattering of k_d (rmse: 21.7 s) compared to k_s (rmse: 2.6 s) during D4 is due to a variable float depth during ZPs. These biased values have been flagged, and interpolated data points were used instead for later data processing. At the end of D4, values of k_d and k_s approach 230 and 161 s, respectively, which is the same for the following deployments until the end of D7.

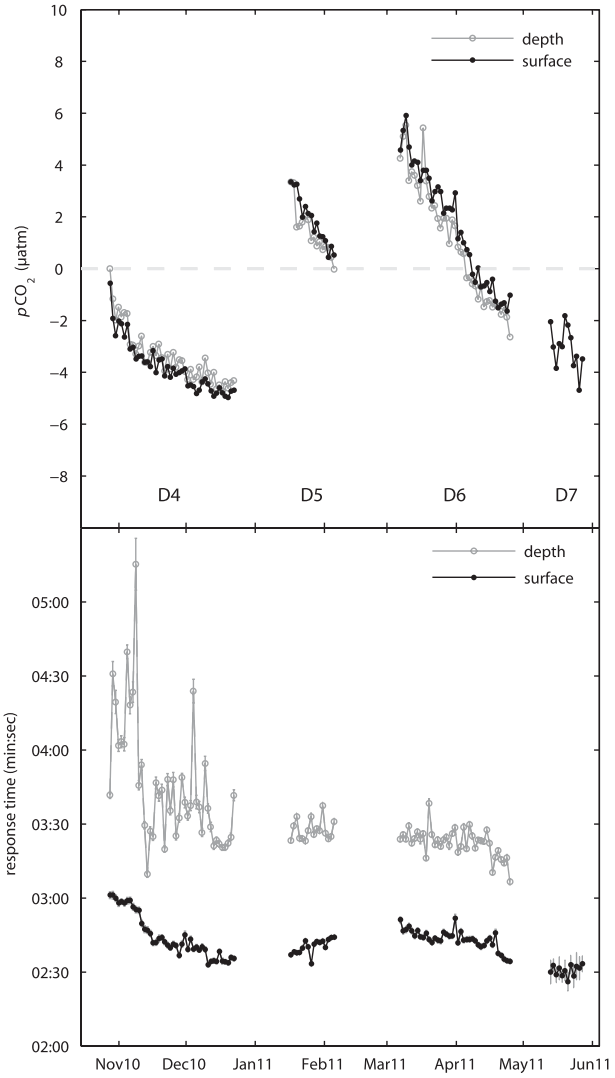

FIG. 2. (top) CO_2 sensor performance in terms of signal stability derived from regular ZPs referred to the first ZP signal (being set to 0 μatm). The ZPs were carried out for a postcompensation of sensor drift that had occurred during the course of deployments. (bottom) In situ response times determined from ZPs. Note: Operation of the CO_2 sensor at the beginning of every profile was slightly changed after D4; therefore, systematic differences between surface and depth ZPs have slightly changed between D4 and the remaining deployments. Further, data at depth for D7 are missing because of the loss of the float.

In contrast to the obvious trends of k_d and k_s during the conditioning period, less pronounced trends are found afterward. Since no overall trend of k_d and k_s is observed, the development of a significant organic film impeding CO_2 permeation can be ruled out. The general

difference between k_d and k_s also must be explained in order to understand CO_2 sensor behavior under different environmental conditions. Since the kinetic response time depends first and foremost on the membrane's permeability, a distinct temperature dependence as found for membrane inlets in other studies (McNeil et al. 2006; Prabhakar et al. 2005) was expected. Indeed, values for k_d and k_s from D5 to D7 show a temperature dependence with ambient water temperature that indicates a linear dependence (Fig. 3). This finding is being corroborated by laboratory tests performed at various water temperatures (data not shown here). Data obtained during the D4 conditioning phase initially fall off this dependency but converge toward and eventually coincide with it too.

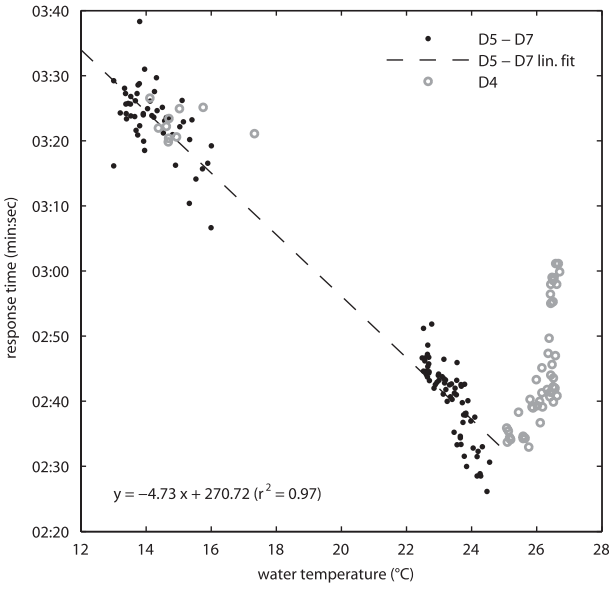

FIG. 3. Observed temperature dependence of sensor response time (k_s and k_d) during all deployments. Gray open circles highlight D4 values, since these deviate significantly from the overall dependence observed during remaining deployments. Inadequate values for k_d (D4) due to variable float depth during ZP were neglected. The equation for the straight line and the correlation coefficient are given in the lower left.

b. CO_2 data consistency

Determined in situ response times described in section 3a are of a magnitude that causes a pronounced hysteresis in the recorded raw sensor data. Using its observed temperature dependence, the sensor's response time can be explicitly calculated for each particular measurement, such that the time-lag correction algorithm described in section 2d can be applied (Fig. 4, right panel). Raw data are carefully smoothed in the time domain according to Miloshevich et al. (2004) without sacrificing much vertical structure (black solid line). TLC data (red solid line) represent the ambient pCO_2 profile.

For the purpose of this study, shipborne field tests were conducted to demonstrate the feasibility of using this sensor in a profiling approach in general and to validate the applicability of the TLC algorithm used. Figure 4 (left and middle panels) shows the results of a HydroC sensor, identical to the unit deployed on the float, being mounted on a CTD rosette sampler while profiling through the upper 500 m of the water column with ascent and descent rates of 0.5 and 0.3 m s^{-1}, respectively. In contrast to the float's measurement routine (right panel, mean ascent rate of 0.06 m s^{-1}) where only upcast data are available, hydrocast data provide both upcasts and downcasts and therefore allow more detailed analysis of the sensor's hysteresis. Recorded raw data (Δt = 2s) have been treated similarly to data obtained by the float, and TLC data were compared for internal consistency between upcasts and downcasts as well as with a set of reference samples collected during the upcasts. Remaining differences between time-lag-corrected upcasts and downcasts are being amplified in case of high ascent and descent rates (up to 60 μatm, left panel) and mainly result from (i) an inadequate modeling of the apparent sensor response time (only very few determinations of k_s and k_d are available) and (ii) a relative decrease of the measurement interval Δt (section 2d) at higher profiling rates. However, slowing down these rates to 0.3 m s^{-1} (middle panel) already produces corrected data that have no systematic offset between upcast and downcast, although deviations still remain significant (particularly in areas of steep gradients). Averaged offsets ($\pm$rmse) of TLC data between upcasts and downcasts for both CTD tests were found to be 10 $\pm$12.4 μatm (0.5 m s^{-1}) and 7.9 $\pm$12 μatm (0.3 m s^{-1}), respectively, which provides a significant improvement compared to non-TLC data (69.8 $\pm$75.7 and 78.3 $\pm$82.9 μatm, respectively). The observed overall consistency for upcasts and downcasts after TLC therefore provides a measure of the quality of data processing procedures and further indicates an increasing precision with slowing ascent and descent rates. In case of floatborne pCO_2 profiles with very slow and varying ascent rates and a well-modeled sensor response time, the above observed deviations are assumed to become almost negligible relative to the measurement accuracy.

The assessment of overall pCO_2 data accuracy turned out to be a rather complicated issue. In contrast to underway measurements at the surface, and therefore the given opportunity to apply established high accuracy methods as a reference (e.g., Körtzinger et al. 1996; Pierrot et al. 2009), no direct and in situ reference

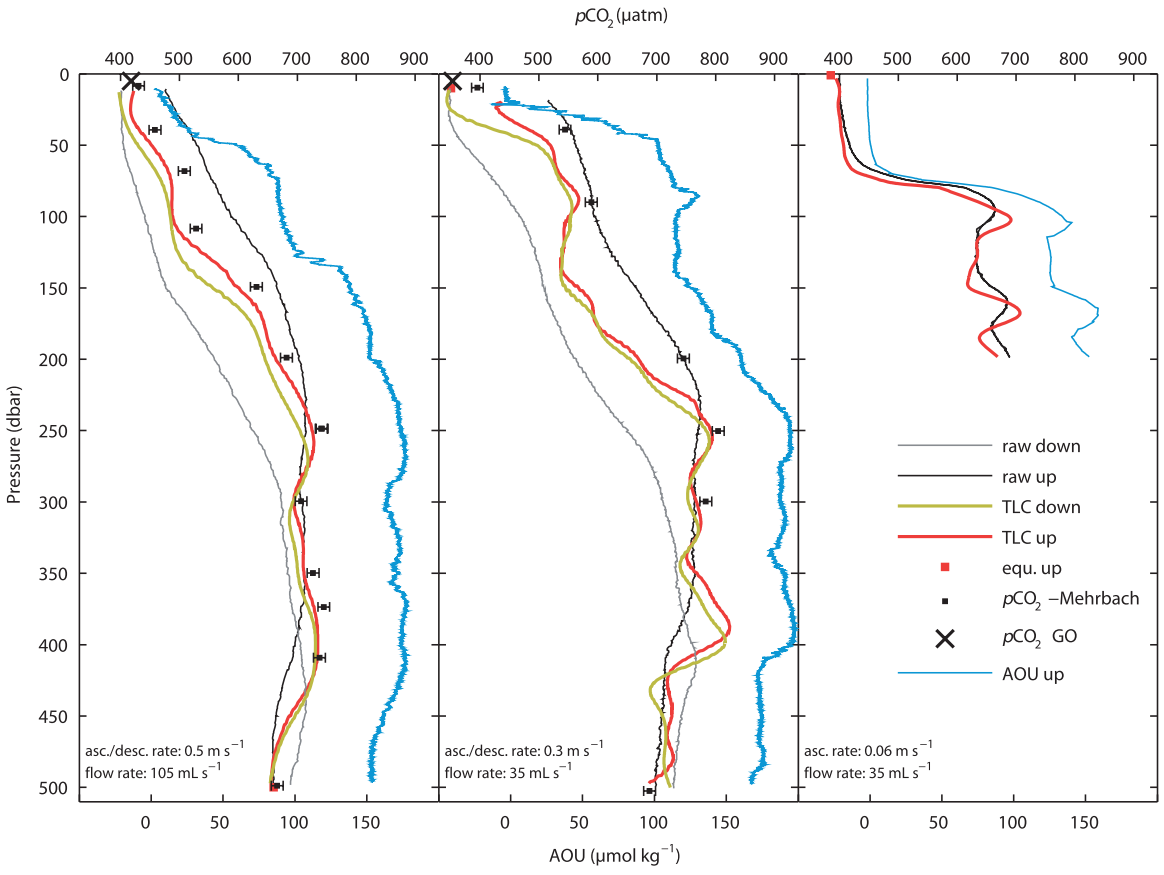

FIG. 4. TLC and original vertical pCO_2 profiles recorded during the hydrographic survey of research vessel (R/V) *Maria S. Merian* (MSM-18/3) with descent rates of (left) 0.5 and (middle) 0.3 m s^{-1}. HydroC was mounted on a CTD rosette sampler, reference samples for pCO_2 (DIC and TA) were taken during the upcast, and surface pCO_2 measurements were performed with a GO underway system (pCO_2, black crosses). Sensor configuration and ascent and descent rates were changed between the casts (see panels). (right) Float upcast recorded during D6 with raw and TLC data. AOU data (blue lines, all panels) represent a qualitative consistency check for the TLC HydroC data. Fully equilibrated (stationary) HydroC sensor signals (red squares, all panels) were achieved after ZPs.

measurements with the required accuracy are available for in situ measurements in the water column. Even pCO_2 values derived from discrete (ex situ) DIC and TA measurements during CTD tests (upcast) still carry an estimated uncertainty of 10 μatm. Further, deviations between these measurements at the surface and an operated underway system (GO) during CTD tests are even above this threshold (Fig. 4, middle panel), pointing at the inadequate matching of these measurements (in space and/or time) and thus indicating an insufficient reliability for this in situ assessment. Despite these constraints, a good overall agreement of TLC data (upcast) with reference samples was found for both hydrocasts in areas of flat gradients (-12.1 ± 5.7 μatm, $n = 10$). Additionally, fully equilibrated pCO_2 sensor data at the surface directly after an upcast (Fig. 4, middle panel) are in good agreement with the underway system (within 3 μatm). Because of the above-described limitations, oxygen measurements [converted to apparent oxygen utilization (AOU)] conducted during CTD tests and float profiles were used to serve as an independent and qualitative proxy of obtained pCO_2 data reliability. In all three cases (Fig. 4), a strong anticorrelation between both gases beneath the mixed layer was found even in the fine vertical structure. These results point at the validity of the applied algorithm as a robust tool for postprocessing of obtained float data.

Postprocessing of time-lagged sensor data removed most of the hysteresis effects; however, other effects on a different time scale still remain in recorded profiles. In particular, TLC data within the mixed layer after an upcast still deviate from final equilibrated values at the end of each upcast (Fig. 4, middle and right panels). This effect could not be fully compensated for by time-lag corrections for pCO_2, and thus it must be caused by other effects on a different time scale. Such effects on measurements could be due to remaining physicochemical influences, such as changes in internal headspace gas

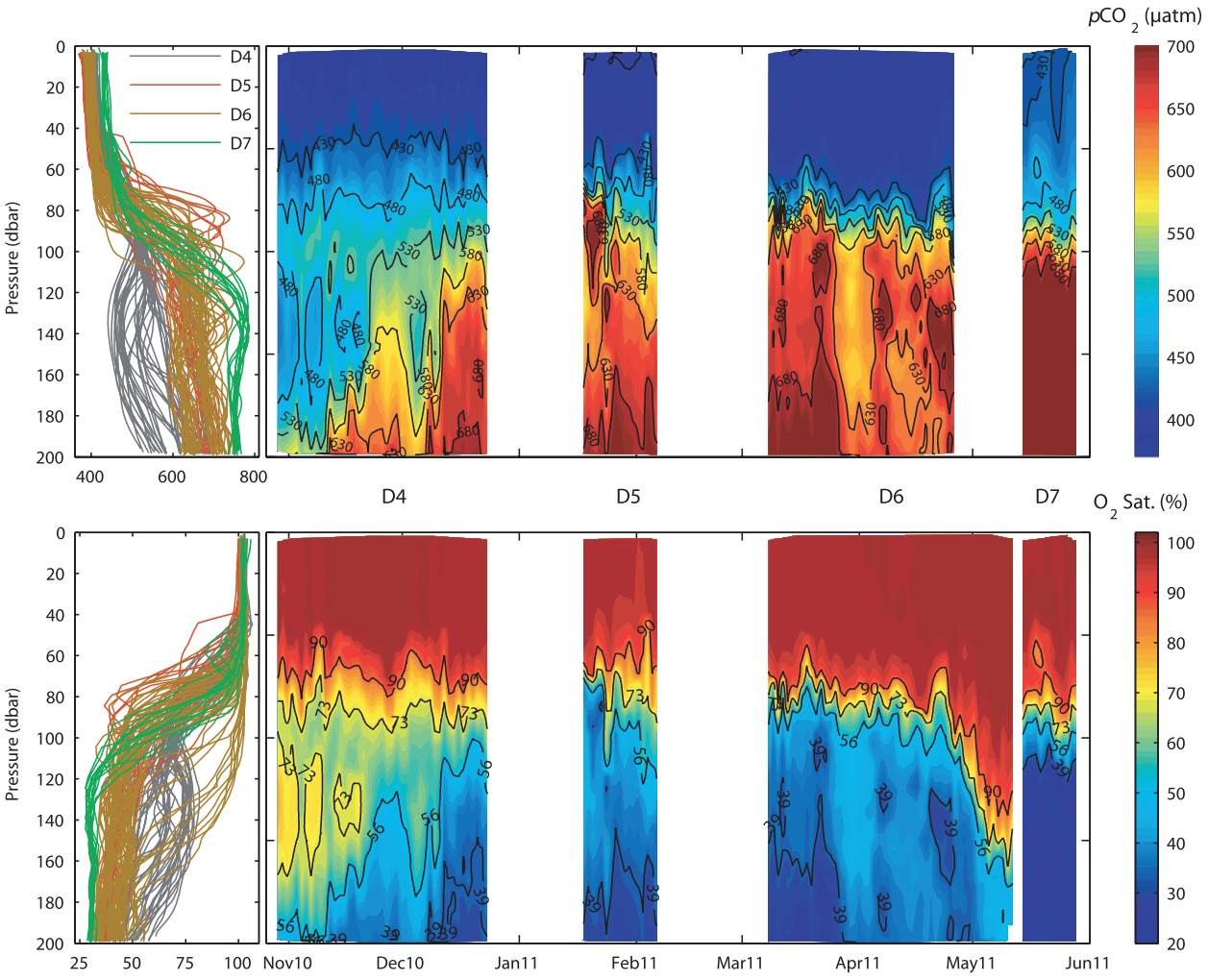

FIG. 5. Final (top) pCO_2 and (bottom) O_2 data collected in the vicinity of CVOO. Time series for both parameters are strongly complementary to each other. Blank areas indicate times when the instrument was refurbished on land–ship for the next deployment. Note: Rapid change in water column properties between D6 and D7 results from the large distance (~280 nm) between recovery and redeployment (see Fig. 1).

temperature and pressure during an upcast or a varying gas matrix composition. The latter might be triggered by steep O_2 gradients in the water column that the sensor experiences during the ascent. Oxygen shows a fivefold reduced permeability for polydimethylsiloxane (PDMS)-type membranes compared to CO_2 (Merkel et al. 2000), and this difference in permeabilities between both gases may result in transient pressure disequilibria that also affect the CO_2 mole fraction during the matrix re-equilibration phase. While equilibration of CO_2 occurs faster than the remaining part of the gas matrix, the measured CO_2 mole fraction xCO_2 might be affected by the slow response of O_2 equilibration. This effect could potentially explain observed deviations in the mixed layer (after the float has passed the oxycline) toward an increased xCO_2 in the sample gas. These dynamic processes at the membrane interface are not fully understood yet, and further experiments in the laboratory and the field are needed to fully understand these transient processes.

All recorded pCO_2 data during D4 and D7 were postprocessed following the validated procedures described in section 2d. Final data (Fig. 5) were found to be tightly anticorrelated for the subsurface and most parts of the surface layers. Some features toward the end of D7, however, show some decoupling in the surface layer. High frequency profiling of the float (every 31 h) allowed to resolve dynamic features in the water column, such as the ventilation of the subsurface layer with low pCO_2 and enhanced O_2 concentrations during D4 or enhanced supersaturation for O_2 and pCO_2 at the end of D7.

To validate TLC pCO_2 data at deployments, pCO_2 reference data (see section 2e) collected either next to

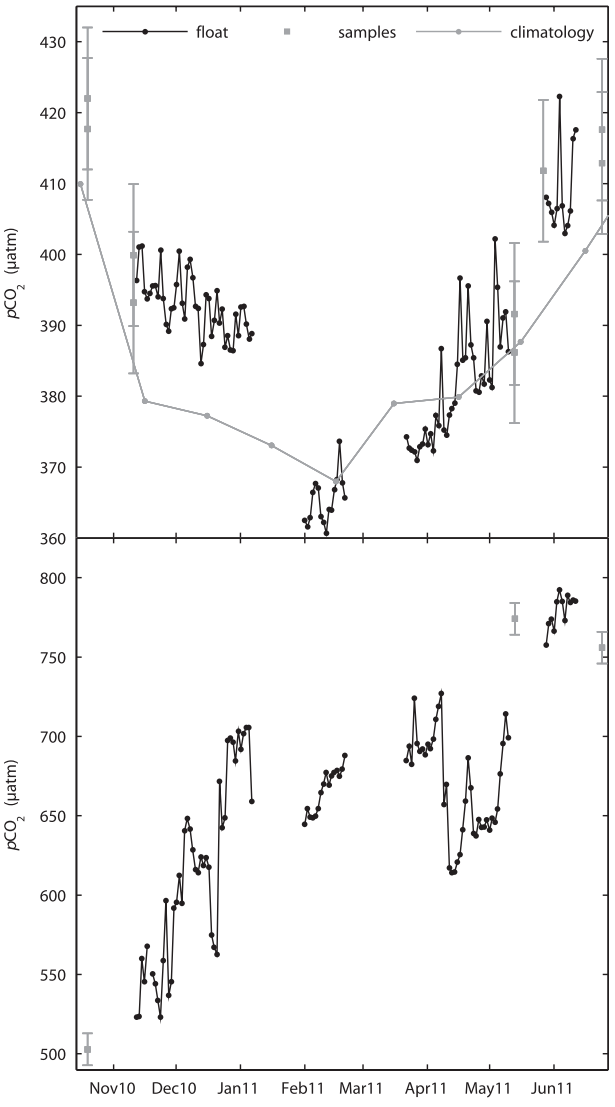

FIG. 6. Floatborne pCO_2 observations at CVOO for the (top) surface ocean (~1 dbar, black solid line) and (bottom) 26.55 sigma-theta isopycnal. Discrete reference samples for pCO_2 were derived from DIC and TA measurements taken in the vicinity of the study area. Climatological pCO_2 values were derived from Takahashi et al. (2009).

the float deployment sites or in the vicinity of CVOO have been used for comparison purposes. Figure 6 shows pCO_2 data from all four deployments for the surface layer (~1 dbar, top panel) and for a density layer (26.55 isopycnal, bottom panel) along the float trajectories. Because of limited sampling capabilities during consecutive deployments and recoveries, no highly resolved vertical profiles for reference samples could be conducted next to float positions. Therefore, only a small number of surface samples and an even smaller set of samples from depth are available for comparison. However, despite lateral displacement all reference samples, both at the surface and at depth, show a good agreement with floatborne observations to within the uncertainty of the calculated pCO_2 (± 10 μatm). Furthermore, climatology data for this particular region and time of year fit well with the seasonal cycle observed by the float. Minor differences could be due to both extrapolation errors of climatology data (from the reference year 2000 to the present) and nonclimatological situations in the field data. Further evidence for robust measurements over the course of all four deployments is given by ZPs illustrated in Fig. 2 (top panel) that followed a very consistent drift pattern. Even though no postdeployment calibration could be realized, the overall agreement with the above named references points at a consistent signal drift even for the response slope. Therefore, ZPs provide an appropriate basis for post-correction of the signal drift encountered during this study.

In summary, all available reference sources provide the evidence for reliable pCO_2 measurements conducted by a profiling float for the first time. The estimated accuracy ranged from 10 to 15 μatm for the water column and 5 μatm for surface measurements.

c. O_2 data consistency

Laboratory-calibrated optode data were treated according to the methods described in section 2d but could not be considered for TLC processing because of inadequately coarse (given the sensor's rather short response time) temporal resolution of measurements. However, the response times of the used optode sensor (18–23 s) observed during laboratory experiments are an order of magnitude faster than the HydroC ones. Thus, an applied time-lag correction would have only an impact of <2 μmol kg^{-1} on oxygen float data in areas of steep O_2 gradients, as being encountered during D4–D7. In absence of such dynamic processes, calibrated optode measurements at the surface did show, however, a discrepancy in reference samples (see below). Therefore, the results of the newly developed approach for an in situ offset correction of biased optode data are being discussed in the following.

The demonstrated long-term stability of optode-based O_2 measurements on unattended platforms is a major advantage of this method, although on most autonomous applications, such as Argo floats, the long-term stability of a given sensor cannot be proven easily. As proposed by Körtzinger et al. (2005), the possibility to measure atmospheric O_2 with the optode sensor can be used as a means of drift control. In this study, five O_2 measurements (quintuplicates) were performed at 90-s intervals in the surface ocean and the overlying air

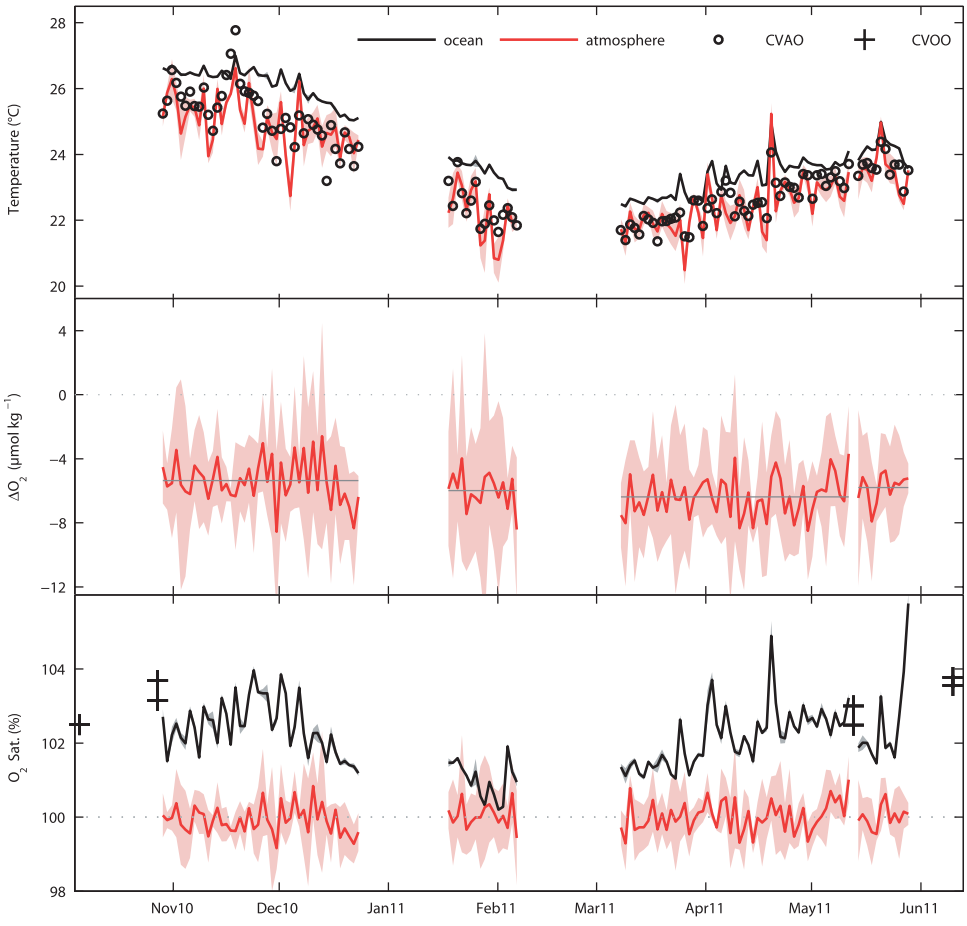

FIG. 7. Temperature and O_2 measurements at the ocean–atmosphere boundary from all four deployments. Shaded areas in all panels give the standard error of the respective property. (top) Temperature readings of the optode sensor in seawater and air as well as air temperature measurements conducted at CVAO. (middle) Differences between measured $O_{2,air}$ and computed $O_{2,air\text{-}calc}$ (see text). Gray lines indicate mean offset for each deployment. (bottom) Calibrated and drift-corrected O_2 saturation levels in the atmosphere (red lines) and in the surface ocean (black lines) with the changing degree of supersaturation. Reference Winkler data (+) were in agreement with corrected optode measurements.

(typically 30 cm above and below the air–sea interface). The resulting precision (rmse for quintuplicates) was found to be 3.2 μmol kg^{-1} for $O_{2,air}$ and 0.3 μmol kg^{-1} for corresponding oxygen measurements in the water ($O_{2,water}$). Weighted means of these measurements are shown in Fig. 7. The elevated noise level of atmospheric O_2 is probably due to rough sea conditions and therefore occasional submersion of the sensor by waves and/or due to a drying sensor foil while measuring in air. However, neither a systematic warming of the sensor in air (due to sunlight) nor a significant cooling (due to evaporation) has been observed (Fig. 7, top panel). The detected mean temperature difference for the optode temperature probe between the surface ocean and atmosphere (1.02 ±0.62°C) is therefore assumed to be real, which is corroborated by land-based measurements at CVAO.

Calibration-based O_2 measurements in air ($O_{2,air}$) underestimate calculated O_2 levels in air at the sea surface ($O_{2,air\text{-}calc}$ after García and Gordon 1992), using an O_2 mixing ratio of 0.20946, and atmospheric pressure and relative humidity, both measured at CVAO. In case no atmospheric in situ data from nearby monitoring sites are available, one could also make use of National Centers for Environmental Prediction (NCEP) reanalysis data (Kanamitsu et al. 2002). However, reported uncertainties in NCEP data (Padin et al. 2007) could negatively affect the accuracy of computed $O_{2,air\text{-}calc}$ and thereby limit this approach. The offset (ΔO_2) between $O_{2,air}$ and $O_{2,air\text{-}calc}$ over time was then used to postcorrect $O_{2,water}$, thereby removing an offset of −5.4 to −6.4 μmol kg^{-1} (rmse: 1.2 μmol kg^{-1}) that slightly varied between consecutive deployments (Fig. 7, middle panel). The change in this offset is very small and not significant. However,

a similar magnitude, sign, and variability of such an offset between deployment and (re) calibration has been observed already during other investigations (Bittig et al. 2012). Taking into account uncertainties of measurements, derived $O_{2,air\text{-}calc}$, and observed stepwise sensor offset, we estimate an overall accuracy of 2 μmol kg^{-1} for floatborne O_2 concentrations in absence of dynamical effects (e.g., time lag). Derived O_2 saturation levels for the topmost part of the mixed layer match well with independent O_2 reference samples (see Fig. 7, bottom panel). Thus, atmospheric measurements during the entire float lifetime appear to provide a valuable tool for in situ drift correction.

Observed O_2 disequilibrium at the ocean–atmosphere interface throughout the deployments (Fig. 7, bottom panel) points at a variability of O_2 that follows a seasonal pattern and a pronounced variability on shorter time scales (e.g., days). Slightly supersaturated waters around CVOO are quite common for this region and even enhanced supersaturation (at the end of D7) can be caused by more productive filaments that are being transported offshore from the Mauritanian upwelling (Fischer et al. 2009).

4. Conclusions

With a new generation of pCO_2 sensors that feature small dimensions and power requirements as well as sufficient precision and accuracy, autonomous pCO_2 measurements become feasible for autonomous profiling applications. In this study we demonstrated the capability of such a sensor being mounted on an Argo-type profiling float for reliable pCO_2 measurements in midterm deployments. First results point at good stability of measurements, absence of biofouling issues and reasonably good agreement with reference data (estimated accuracy: 5 μatm for surface measurements and 10–15 μatm in profiling mode). Because of the slow sensor response time, a postprocessing of profiling pCO_2 data is crucial for obtaining unbiased profiles. Such a correction algorithm was validated by extended field tests of the HydroC sensor on a water sampling rosette and applied successfully to reconstruct ambient pCO_2 profiles from time-lagged sensor data. Optode-based O_2 measurements made directly at the ocean–atmosphere boundary provide valuable results for an accurate drift correction of optode data (within 2 μmol kg^{-1} in absence of dynamic effects) and therefore enable precise air–sea gas exchange studies.

Future improvements of the pCO_2 sensor, as well as increasing the pumped water flow on the float platform by a stronger pump (SBE 5P pump, ~5.4 W instead of SBE 5M, ~1.8 W), clearly have the potential to further reduce the sensor's response time and hence minimize the magnitude of time-lag correction. Thus, accuracy and precision of measurements from profiling or moving platforms can likely be further improved.

Adaption of the presented measurement approach toward an Argo-like mission without redeployments could be made possible in the future. The conducted midterm deployments have demonstrated reliable pCO_2 measurements with a comprehensible drift pattern that could be monitored and accounted for. In addition, promising ongoing developments of the HydroC toward reduced sensor size and energy consumption could significantly extend possible deployment times. Further improvements of the NEMO platform, such as higher battery or sensor payload capacity, also help increase deployment duration and thereby enable long-term deployments for this sensor suite. A fair balance between deployment duration, sampling interval, energy consumption, and accuracy demands has to be assessed for future deployment needs.

The feasibility of combined pCO_2 and O_2 measurements on an autonomous profiling platform has successfully been shown within this work, even though new methodological questions for future investigations have to be addressed (e.g., potential gas matrix effects on pCO_2 data). However, these results demonstrate the potential for this type of measurement for future detailed autonomous investigations of O_2 and carbon dynamics in both the ocean's interior and the ocean–atmosphere boundary layer.

Acknowledgments. The authors thank Ivanice Monteiro and Carlos Santos from the Instituto Nacional de Desenvolvimento das Pescas (INDP) in Mindelo, Cape Verde, as well as the entire crew of R/V *Islândia* for their tremendous support of the field work conducted at CVOO. We further thank the team of Optimare GmbH (Timo Witte, Michael Busack, Günter Buss, Oliver Zenk, Harald Rohr, and Barbara Cembella) for their passionate and professional work on the construction of the prototype float(s). Thanks are also due to CONTROS personnel who have supported the endeavor of measuring pCO_2 profiles on a profiling float and to Sebastian Fessler and Tobias Steinhoff for the analysis of reference samples. Acknowledgement is made to the Facility for Ground-Based Atmospheric Measurement (FGAM) and the National Centre for Atmospheric Science (NCAS) for the use of the Cape Verde Atmospheric Observatory meteorological data. We also like to thank Larry Miloshevich for his helpful comments on the time-lag corrections. This work was funded by the German Federal Ministry of Education and Research under the SOPRAN project (Grants 03F0462A and 03F0611A).

REFERENCES

Baudot, A., I. Souchon, and M. Marin, 1999: Total permeate pressure influence on the selectivity of the pervaporation of aroma compounds. *J. Membr. Sci.,* **158,** 167–185.

Bishop, J. K. B., T. J. Wood, R. E. Davis, and J. T. Sherman, 2004: Robotic observations of enhanced carbon biomass and export at 55°S during SOFeX. *Science,* **304,** 417–420.

Bittig, H. C., B. Fiedler, T. Steinhoff, and A. Körtzinger, 2012: A novel electrochemical calibration setup for oxygen sensors and its use for the stability assessment of Aanderaa optodes. *Limnol. Oceanogr. Methods,* **10,** 921–933.

Boss, E., D. Swift, L. Taylor, P. Brickley, R. Zaneveld, S. Riser, M. J. Perry, and P. G. Strutton, 2008: Observations of pigment and particle distributions in the western North Atlantic from an autonomous float and ocean color satellite. *Limnol. Oceanogr.,* **53,** 2112–2122.

Boutin, J., and L. Merlivat, 2009: New in situ estimates of carbon biological production rates in the Southern Ocean from CARIOCA drifter measurements. *Geophys. Res. Lett.,* **36,** L13608, doi:10.1029/2009GL038307.

Byrne, R. H., and Coauthors, 2010: Sensors and systems for in situ observations of marine carbon dioxide system variables. *Proceedings of OceanObs'09: Sustained Ocean Observations and Information for Society,* J. Hall, D. E. Harrison, and D. Stammer, Eds., Vol. 2, ESA Publ. WPP-306, doi:10.5270/OceanObs09.cwp.13.

D'Asaro, E., and C. McNeil, 2007: Air–sea gas exchange at extreme wind speeds measured by autonomous oceanographic floats. *J. Mar. Syst.,* **66,** 92–109, doi:10.1016/j.jmarsys.2006.06.007.

Davis, R. E., J. T. Sherman, and J. Dufour, 2001: Profiling ALACEs and other advances in autonomous subsurface floats. *J. Atmos. Oceanic Technol.,* **18,** 982–993.

DeGrandpre, M. D., T. R. Hammar, S. P. Smith, and F. L. Sayles, 1995: In-situ measurements of seawater pCO_2. *Limnol. Oceanogr.,* **40,** 969–975.

Dickson, A. G., 2010: Standards for ocean measurements. *Oceanography,* **23,** 34–47.

——, and F. J. Millero, 1987: A comparison of the equilibrium constants for the dissociation of carbonic acid in seawater media. *Deep-Sea Res. I,* **34,** 1733–1743, doi:10.1016/0198-0149(87)90021-5.

Dore, J. E., R. Lukas, D. W. Sadler, and D. M. Karl, 2003: Climate-driven changes to the atmospheric CO_2 sink in the subtropical North Pacific Ocean. *Nature,* **424,** 754–757.

Eckles, R. D., J. M. Welles, and K. Peterson, 1993: CO_2 and CO_2/H_2O infrared gas analyzers. *Meas. Control,* **161,** 83–89.

Edwards, B., D. Murphy, C. Janzen, and N. Larson, 2010: Calibration, response, and hysteresis in deep-sea dissolved oxygen measurements. *J. Atmos. Oceanic Technol.,* **27,** 920–931.

Fietzek, P., S. Kramer, and D. Esser, 2011: Deployment of the HydroC (CO_2/CH_4) on stationary and mobile platforms - Merging the trends in the field of platform and sensor development. *Proc. Oceans '11 MTS/IEEE Kona,* Waikoloa, Hawaii, MTS and IEEE/EOS, 9 pp.

Fischer, G., C. Reuter, G. Karakas, N. Nowald, and G. Wefer, 2009: Offshore advection of particles within the Cape Blanc filament, Mauritania: Results from observational and modelling studies. *Prog. Oceanogr.,* **83,** 322–330, doi:10.1016/j.pocean.2009.07.023.

García, H. E., and L. I. Gordon, 1992: Oxygen solubility in seawater: Better fitting equations. *Limnol. Oceanogr.,* **37,** 1307–1312.

Gruber, N., J. L. Sarmiento, and T. F. Stocker, 1996: An improved method for detecting anthropogenic CO_2 in the oceans. *Global Biogeochem. Cycles,* **10,** 809–837.

——, and Coauthors, 2010a: Adding oxygen to Argo: Developing a global in-situ observatory for ocean deoxygenation and biogeochemistry. *Proceedings of OceanObs'09: Sustained Ocean Observations and Information for Society,* J. Hall, D. E. Harrison, and D. Stammer, Eds., ESA Publ. WPP-306, doi:10.5270/OceanObs09.cwp.39.

——, and Coauthors, 2010b: Toward an integrated observing system for ocean carbon and biogeochemistry at a time of change. *Proceedings of OceanObs'09: Sustained Ocean Observations and Information for Society,* J. Hall, D. E. Harrison, and D. Stammer, Eds., ESA Publ. WPP-306, doi:10.5270/OceanObs09.pp.18.

Johnson, K. M., J. M. Sieburth, P. J. L. Williams, and L. Brändström, 1987: Coulometric total carbon dioxide analysis for marine studies: Automation and calibration. *Mar. Chem.,* **21,** 117–133.

Johnson, K. S., S. C. Riser, and D. M. Karl, 2010: Nitrate supply from deep to near-surface waters of the North Pacific subtropical gyre. *Nature,* **465,** 1062–1065, doi:10.1038/nature09170.

Kanamitsu, M., W. Ebisuzaki, J. Woollen, S.-K. Yang, J. J. Hnilo, M. Fiorino, and G. L. Potter, 2002: NCEP–DOE AMIP-II Reanalysis (R-2). *Bull. Amer. Meteor. Soc.,* **83,** 1631–1643.

Keeling, R. F., A. Körtzinger, and N. Gruber, 2010: Ocean deoxygenation in a warming world. *Annu. Rev. Mar. Sci.,* **2,** 199–229, doi:10.1146/annurev.marine.010908.163855.

Körtzinger, A., H. Thomas, B. Schneider, N. Gronau, L. Mintrop, and J. C. Duinker, 1996: At-sea intercomparison of two newly designed underway pCO_2 systems – Encouraging results. *Mar. Chem.,* **52,** 133–145.

——, J. Schimanski, U. Send, and D. Wallace, 2004: The ocean takes a deep breath. *Science,* **306,** 1337, doi:10.1126/science.1102557.

——, ——, and ——, 2005: High quality oxygen measurements from profiling floats: A promising new technique. *J. Atmos. Oceanic Technol.,* **22,** 302–308.

——, and Coauthors, 2008: The seasonal pCO_2 cycle at 49°N/16.5°W in the northeastern Atlantic Ocean and what it tells us about biological productivity. *J. Geophys. Res.,* **113,** C04020, doi:10.1029/2007JC004347.

Marin, M., K. Kalantzi, and H. Gibert, 1992: Pervaporation process: Membrane conditioning and experimental mass transfer analysis. *J. Membr. Sci.,* **74,** 105–114.

McDermitt, D. K., R. D. Eckles, G. L. Biggs, and J. M. Welles, 1993: Effects on temperature and pressure on CO_2 infrared absorption with special emphasis on problems resulting from operation at high flow rates. LI-COR Inc. Application Note 117, 12 pp.

McNeil, C., E. D'Asaro, B. Johnson, and M. Horn, 2006: A gas tension device with response times of minutes. *J. Atmos. Oceanic Technol.,* **23,** 1539–1558.

Mehrbach, C., C. H. Culberso, J. E. Hawley, and R. M. Pytkowic, 1973: Measurement of apparent dissociation constants of carbonic acid in seawater at atmospheric pressure. *Limnol. Oceanogr.,* **18,** 897–907.

Merkel, T. C., V. I. Bondar, K. Nagai, B. D. Freeman, and I. Pinnau, 2000: Gas sorption, diffusion, and permeation in poly(dimethylsiloxane). *J. Polym. Sci.,* **38B,** 415–434.

Millero, F. J., 2007: The marine inorganic carbon cycle. *Chem. Rev.,* **107,** 308–341, doi:10.1021/cr0503557.

Miloshevich, L. M., A. Paukkunen, H. Vömel, and S. J. Oltmans, 2004: Development and validation of a time-lag correction for

Vaisala radiosonde humidity measurements. *J. Atmos. Oceanic Technol.,* **21,** 1305–1327.

Mintrop, L., F. F. Perez, M. Gonzalez-Davila, M. J. Santana-Casiano, and A. Körtzinger, 2000: Alkalinity determination by potentiometry: Intercalibration using three different methods. *Cienc. Mar.,* **26,** 23–37.

Moore, T. S., M. D. DeGrandpre, C. L. Sabine, R. C. Hamme, C. J. Zappa, W. R. McGillis, R. A. Feely, and W. M. Drennan, 2011: Sea surface pCO_2 and O_2 in the Southern Ocean during the austral fall, 2008. *J. Geophys. Res.,* **116,** C00F11, doi:10.1029/2010JC006560.

Padin, X. A., M. Vázquez-Rodríguez, A. F. Rios, and F. F. Pérez, 2007: Atmospheric CO_2 measurements and error analysis on seasonal air–sea CO_2 fluxes in the Bay of Biscay. *J. Mar. Syst.,* **66,** 285–296, doi:10.1016/j.jmarsys.2006.05.010.

Pfeil, B., and Coauthors, 2012: A uniform, quality controlled Surface Ocean CO_2 Atlas (SOCAT). *Earth Syst. Sci. Data Discuss.,* **5,** 735–780, doi:10.5194/essdd-5-735-2012.

Pierrot, D., and Coauthors, 2009: Recommendations for autonomous underway pCO_2 measuring systems and data-reduction routines. *Deep-Sea Res. II,* **56,** 512–522, doi:10.1016/j.dsr2.2008.12.005.

Prabhakar, R. S., R. Raharjo, L. G. Toy, H. Lin, and B. D. Freeman, 2005: Self-consistent model of concentration and temperature dependence of permeability in rubbery polymers. *Ind. Eng. Chem. Res.,* **44,** 1547–1556, doi:10.1021/ie0492909.

Riser, S. C., and K. S. Johnson, 2008: Net production of oxygen in the subtropical ocean. *Nature,* **451,** 323–325, doi:10.1038/nature06441.

Roemmich, D., G. Johnson, S. Riser, R. Davis, and J. Gilson, 2009: The Argo program: Observing the global ocean with profiling floats. *Oceanography,* **22,** 34–43.

Stephens, B. B., R. F. Keeling, M. Heimann, K. D. Six, R. Murnane, and K. Caldeira, 1998: Testing global ocean carbon cycle models using measurements of atmospheric O_2 and CO_2 concentration. *Global Biogeochem. Cycles,* **12,** 213–230, doi:10.1029/97GB03500.

Stramma, L., and F. Schott, 1999: The mean flow field of the tropical Atlantic Ocean. *Deep-Sea Res. II,* **46,** 279–303.

Takahashi, T., and Coauthors, 2009: Climatological mean and decadal change in surface ocean pCO_2, and net sea–air CO_2 flux over the global oceans. *Deep-Sea Res. II,* **56,** 554–577, doi:10.1016/j.dsr2.2008.12.009.

Tengberg, A., and Coauthors, 2006: Evaluation of a lifetime-based optode to measure oxygen in aquatic systems. *Limnol. Oceanogr. Methods,* **4,** 7–17.

Uchida, H., T. Kawano, I. Kaneko, and M. Fukasawa, 2008: In situ calibration of optode-based oxygen sensors. *J. Atmos. Oceanic Technol.,* **25,** 2271–2281.

Watson, A. J., and Coauthors, 2009: Tracking the variable North Atlantic sink for atmospheric CO_2. *Science,* **326,** 1391–1393, doi:10.1126/science.1177394.